Telecommunications and Radio Engineering, 79(20):1-12 (2020)

RADIO TECHNOLOGY IN BIOMEDICAL INVESTIGATION

AUTOMATED DETECTION OF PATHOLOGICAL AND NON-PATHOLOGICAL MYOPIA USING RETINAL FEATURES AND DYNAMIC ENSEMBLE OF CLASSIFIERS

S. Pathan,* P.C. Siddalingaswamy, & N. Dsouza

Manipal Institute of Technology, Manipal Academy of Higher Education, Manipal, Karnataka 576104, India

*Address all correspondence to: S. Pathan, E-mail: sameena.pathan.k@gmail.com

A computer-aided diagnostic tool for myopia detection is of paramount importance since the pathology results in irreversible damage to the eye. Unfortunately, designing of such systems is hindered by several issues such as (i) difficulties in segmentation of optic disc (OD) due to smooth variability between the OD and other retinal features, (ii) greater degree of correlation between myopia and non-myopic features, and (iii) lack of feasibility for adopting in a clinical setting. The proposed methodology is designed to address the aforementioned issues. First, blood vessels are detected and excluded. Second, the optic disc region is segmented using deformable models. Further, two classification set-ups are tested to determine the rate of accurate classification to detect myopia. Quantitative analysis is performed on the PALM dataset achieving, sensitivity, specificity, and accuracy of 90.3 %, 100 %, and 95 % respectively.

KEY WORDS: *myopia, pathological myopia, ensemble classifiers, multilayer perceptron, shape, color, texture*

1. INTRODUCTION

Myopia is considered the most prevalent eye condition around the globe with a 33 % increase in the cases over in 2020 [1]. Figure 1 illustrates the statics associated with myopia. As the severity of myopia increases certain pathological changes such as macular degeneration, optic disc (OD) changes, posterior staphyloma can be observed [2]. Clinically individuals affected by myopia suffer from blurred images since the reflection focus falls ahead of the retina rather than on the retina. Pathological myopia

is considered as one of the forms of myopia leading to blindness due to posterior segment elongation of the eye. Since the pathologies associated with myopia are irreversible, there is an increased need for early diagnosis. Clinically prevalent methods are subjective in nature, thus motivating the need for an objective CAD tool for early diagnosis. Figure 2 illustrates the normal and pathological myopia affected fundus image.

A PAMELA system was proposed by Liu et al [3] by the detection of parapapillary atrophy changes around the OD region. Zhang et al [2] used a fusion of clinical and essential features to identify myopic fundus images. Multiple kernel learning methods were used by Zhang et al [4] to design a computer-aided diagnostic framework for the detection of pathological myopia.

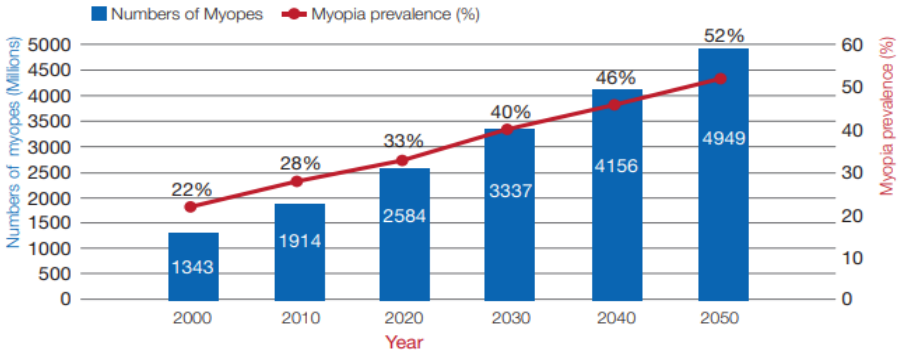

FIG. 1: Myopia prevalence statistics around the globe [1]

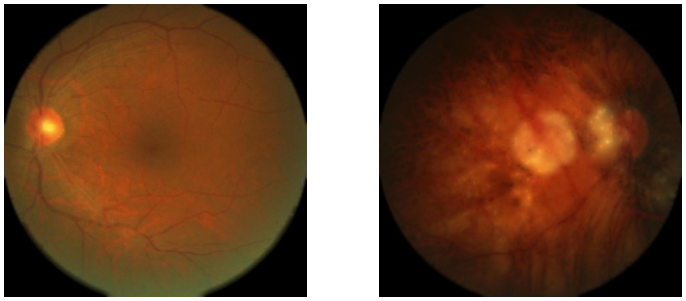

a) b)

FIG. 2: Illustration of normal (a) and diseased (b) fundus images [5]

Pathological myopia is defined by the presence of myopic maculopathy and posterior staphyloma, leading to irreversible and uncorrected visual impairment [6]. OD tilting, retinal tear and detachment, and fundus tessellation are the morphological and pathological changes occurring due to pathological myopia. Due to weaker and thinner lamina tissue, myopic eyes have increased the risk of developing glaucoma

[7,8]. Optic nerve head changes due to myopia hinder the detection of glaucoma [9,10].

The proposed methodology proposes a framework for the detection of pathological myopia and differs from the literature in the following ways.

- Effective blood vessel detection and exclusion.
- Clinical and global image features are used for distinguishing pathological myopia and non-myopic images.

2. MATERIALS AND METHODS

The proposed methodology for the detection of pathological myopia consists of four sequential steps as follows: Blood vessel detection and exclusion, localization of OD, extraction of features such as shape and color features from the OD, and the entire image respectively followed by classification. Two classification set-ups were used for the identification of myopic fundus images. Figure 3 illustrates the detailed methodology for the classification of pathological myopia and normal fundus images. The first part of the block consists of blood vessel detection and exclusion since retinal vessels form a major artifact for studying the properties and pathological changes in the optic disc. The second step includes the segmentation of the optic disc to study the shape characteristics of the OD. Subsequently, shape, color, and texture features are computed from the OD and the fundus images to study specific properties of the myopic fundus images. The classification forms the last stride of the CAD tool. The following sections provide an explanation of the methods proposed for developing the CAD tool.

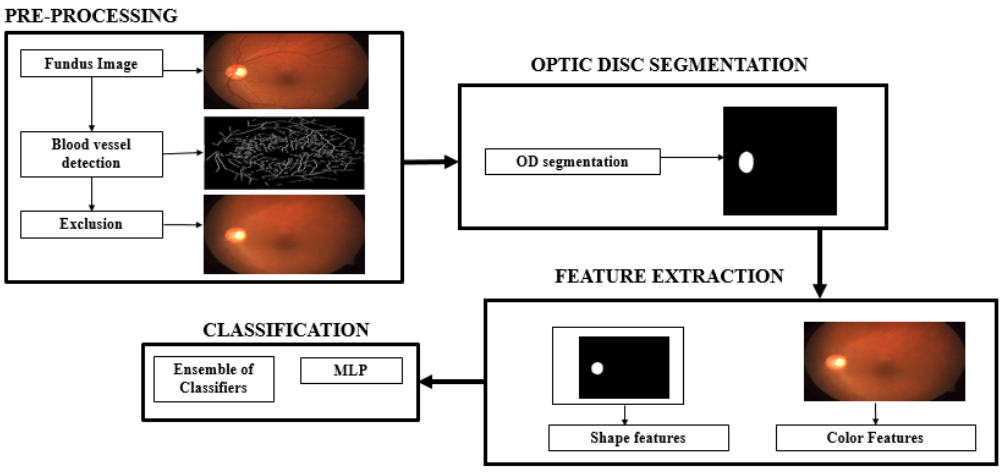

FIG.3: Overview of the proposed system

2.1 Dataset

The dataset consists of annotated 400 fundus images, of which 187 belong to non-pathological myopia and 213 belong to pathological myopia. The non-pathological myopia fundus images consist of images belonging to the category of high myopia and normal.

2.2 Blood Vessel Detection and Exclusion

To detect the optic disk, the retinal vessels are initially segmented and extricated from the fundus image for further processing. Algorithm 1 provides a detailed description of the proposed method for vessel segmentation and exclusion. Initially, the green channel of the RGB image is chosen, since the vessels are prominently visible in the green channel as seen in Fig. 4(b). Further, the image is sharpened to highlight the fine details using a second-order derivative Laplacian filter. Prior to sharpening the green channel of the RGB image is smoothened using a 5×5 average filter. Subsequently, the Laplacian filtered image and the average filtered image are subtracted to yield a sharpened image. Consequently, the sharpened image is subjected to iterations of open and close morphological operations as illustrated in Algorithm 1. The response image is subjected to Otsu thresholding [11] to obtain the mask of the extracted blood vessels. A region fill based inpainting using the mask and the fundus image yields the blood vessel excluded fundus image. A graphical illustration of the results of blood vessel detection exclusion is given in Fig. 4.

ALGORITHM 1: Blood vessel detection and exclusion

Input: $I(x,y)=\{R(x,y),G(x,y),B(x,y)\}$.

Output: $I'(x,y)=Blood\ vessel\ excluded\ fundus\ image$

1. $I_{avg}=Filter_{avg}\{G(x,y),[5,5]\}$
2. $I_{lap}=Filter_{lap}\{G(x,y)\}$
3. $I_{sharp}=I_{lap}-I_{avg}$
4. $I_1=I_{Bothat}\{I_{sharp},line(0,15)\}$
5. $I_2=I_{Bothat}\{I_{sharp},line(15,45)\}$
6. $I_3=I_{Bothat}\{I_{sharp},line(90,15)\}$
7. $I_4=I_{Bothat}\{I_{sharp},line(135,15)\}$
8. $I_5=I_{Bothat}\{I_{sharp},line(180,15)\}$
9. $I_6=I_{Bothat}\{I_{sharp},line(225,15)\}$
10. $I_7=I_{Bothat}\{I_{sharp},line(270,15)\}$
11. $I_8=I_{Bothat}\{I_{sharp},line(315,15)\}$

12. $I_t(x,y) = Add\{I_1 + I_2 + I_3 + I_4 + I_5 + I_6 + I_7 + I_8\}$
13. $t = Otsuthresh(I_t(x,y))$
14. $M(x,y) = \{I_t(x,y), t\}$
15. $I'(x,y) = Region\ fill\{M(x,y), I(x,y)\}$

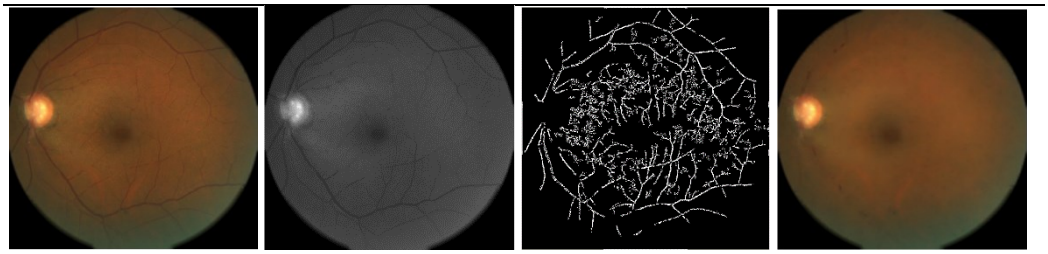

a) b) c) d)

FIG. 4: Results of retinal blood vessel detection and exclusion: fundus image (a), green channel (b, extracted blood vessels (c), and fundus image with excluded blood vessel (d)

2.3 Optic Disc Localization

The blood vessel excluded fundus image is subjected to segmentation using the deformable model to segment the optic disk. The blood vessel excluded fundus images henceforth referred to as fundus images are transformed to CIE-XYZ color space. The X channel is further used for segmenting the OD since the OD is clearly visible in the X channel in comparison to the Y and Z counterparts. Further, the X channel of the image is subtracted from the maximum intensity value of the channel, to highlight the OD region. The image is further thresholded using the non-zero minimum value of the X channel. The mask obtained is used as the initial contour for segmentation. The basic idea of Chan-Vese is to partition the given image $I(x)$into the foreground and background as given in (1) [12].

$$E = \lambda_1 \int (I(x) - c1)^2 dx + \lambda_2 \int (I(x) - c2)^2 dx + \mu\, length(C) + v\, Area(C), \qquad (1)$$

where $\lambda_1, \lambda_2, \mu, v$ are fixed parameters as given in [12]. Using the level set to represent curve C, the zero level set of a Lipschitz function $\varnothing(x)$, the unknown variable C is replaced by $\varnothing(x)$ and the energy function is re-written as given in (2). The parameters in equation (2) are described in detail in (2).

$$\begin{aligned} E = \lambda_1 \int (I(x) - c1)^2 H(\varnothing(x))dx + \lambda_2 \int (I(x) - c2)^2 (1 - H(\varnothing(x)))dx + \\ + \mu \int \delta(\varnothing(x)) |\nabla \varnothing(x)| dx + v \int H(\varnothing(x))dx, \end{aligned} \qquad (2)$$

where $H(\varnothing)$ and $\delta(\varnothing)$ are Heaviside and Dirac functions written as in (3).

$$H(\varnothing)=\frac{1}{2}\left(1+\frac{2}{\pi}\arctan\left(\frac{z}{\varepsilon}\right)\right),$$
$$\delta(\varnothing)=\frac{1}{\pi}\frac{\varepsilon}{\varepsilon^2+z^2}. \tag{3}$$

The results of curve deformation and OD segmentation is given in Fig. 5.

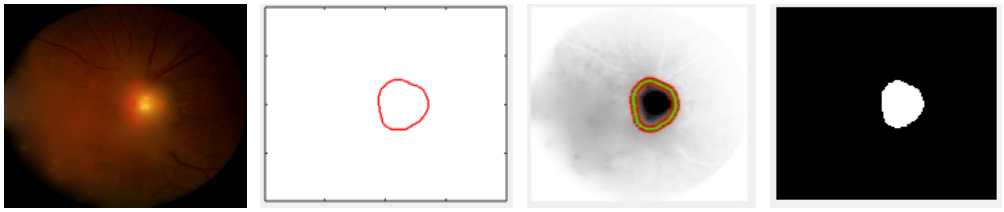

a) b) c) d)

FIG. 5: Segmentation of OA: original image (a), initial contour (b), deformation (c), and segmented mask (d)

2.3 Feature Extraction

2.3.1 Shape Features

A set of seven shape features were computed from the OD. These include the area of the OD, the perimeter of the OD, circularity index, and OD irregularity. The irregularity of the OD is computed by determining the shortest and the longest diameter of the OD region as given in (4)-(7)

$$I_1=\frac{P}{A}, \tag{4}$$
$$I_2=\frac{P}{GD}, \tag{5}$$
$$I_3=P\left(\frac{1}{SD}-\frac{1}{GD}\right), \tag{6}$$
$$I_4=SD-GD, \tag{7}$$

where P is the perimeter, A is the area, GD and SD are the greatest and shortest diameters.

2.3.2 Color Features

A set of three-color features were computed from the fundus image. These include color correlation, color entropy, and color variance. Color correlation- The color correlation is the Pearson's correlation between the red (r), green (g), blue (b), and the grayscale (k) image. Entropy is a measure of the degree of randomness. The degree of randomness with respect to each channel is computed. Similarly, color variance is computed for the red, green, blue, and gray channels of the fundus image. Including the shape and color features a set of 21 features were extracted to analyze the pathologies associated with myopia.

2.4 Lesion Classification

The ultimate step in a CAD system is diagnosis or decision making performed by a classifier. Different classifiers make different errors based on the test sample. In most of the cases, a single classifier is trained and used for testing the test samples. However, this causes generalization error and results in lower classification accuracy. If we create an ensemble of classifiers and dynamically select a classifier depending on the characteristics of the test pattern, then we can reduce the risk of generalization and over-fitting and simultaneously improve the classification accuracy. In this regard, the major concern would be how to dynamically select the classifier depending on the characteristics of the test pattern. This is performed by dynamic ensemble selection techniques [13,14].

The proposed methodology is built using two set-ups, (i) the first model is a multilayer perceptron built using 10 hidden layers, (ii) the second model is built by creating an ensemble of AdaBoost classifiers built using weak learners by bagging.

The first model multilayered perceptron is built using 10 hidden layers and a hyperbolic tangent function. The gradient descent backpropagation algorithm is employed in the multilayered feed-forward network.

The second model is built by creating an AdaBoost of classifiers built using weak learners. Further, the eight classifier selection techniques applied to the two classification models are as follows: The first two techniques (Normal and Ensemble) are the conventional techniques. The first technique termed as "Normal" refers to a single classifier set-up, in the case of the first model, it refers to a single decision stump tree. In the case of the second model, "Normal" refers to a single classifier created by boosting. Static Ensemble here onwards referred as Ensemble refers to a group of decision stump trees created. The number of decision stump trees is decided based on the number of input features. In the case of the first model, a group of decision stump trees is built by bagging. In the case of the second model, a group of decision stump trees is created by boosting. The maximum depth of the tree is two. OLA, LCA, A-Priori, A-Posteriori, KNORA-E, and KNORA-U are dynamic ensemble selection techniques applied to the two classification models. In general, to apply dynamic ensemble selection techniques for a given test pattern, K-nearest neighbors (KNN, here K=5) of the test pattern are chosen from the training samples. This is followed by testing the K-NN training samples using the two ensemble classification models. The procedure for selecting K-NN training samples and the classifier for

classifying each of the test patterns is decided by the dynamic ensemble selection techniques (OLA, LCA, A-Priori, A-Posteriori, KNORA-E, and KNORA-U). Specifically, in the case of OLA, the K-NN training samples chosen for a given test pattern may not have the same class as that of the test pattern. Further, the training process is followed by testing the two ensemble classification models on the K-NN training samples. The classifier that accurately classifies the maximum number of K-NN training samples is chosen to classify the test pattern. If there is more than one classifier that accurately classifies the maximum number of K-NN training samples, then the value of K is increased until a single classifier is obtained. The process is repeated for the entire testing data. In the case of LCA, K-NN training samples should have the same class as the test pattern. A-Priori and A-Posterior are similar to OLA and LCA, here the classifier accuracy is measured in terms of probability of accurate classification. KNORA-E creates an ensemble of classifiers that correctly classify all the K-NN training samples, which is further used for testing the test pattern. Since an ensemble of classifiers is created adaptively for each test pattern, the class of the test pattern is decided using majority voting. KNORA-U creates an ensemble of classifiers that are able to classify at least one of the K-NN training samples for a given test pattern followed by determining the class of the test pattern using majority voting. Subsequently, as the pool of classifiers is built using bagging, dynamic selection techniques are applied to select a classifier for a particular test pattern.

3. RESULTS AND DISCUSSIONS

3.1 Results of Classification using ANN

The set-up was used for evaluating the classification ability for the features extracted.

Set-up 1: In the case of this set-up, 80% of the data was used for training and 20% was used for testing [15]. Each time the samples in the hold-out set vary, and thus the average performance of three iterations is reported. The performance metrics are sensitivity, specificity, and accuracy as given in (8)-(10). Sensitivity (SE) indicates the rate of correct classification of myopia affected eye. Specificity (SP) indicates the rate of correct classification of the normal eye. Accuracy (ACC) indicates the overall correct classification rate.

$$SE = \frac{TP}{FN + TP}, \tag{8}$$

$$SP = \frac{TN}{FP + TN}, \tag{9}$$

$$ACC = \frac{TN + TP}{FN + FP + TN + TP}. \tag{10}$$

True Positive (*TP*): The model accurately predicts that the fundus image is myopic.

True Negative (*TN*): The model accurately predicts that the fundus image is non-myopic.

False Positive (*FP*): The model predicts that the fundus image is non-myopic when it is myopic.

False Negative (*FN*): The model predicts that the fundus image is myopic when it is non-myopic.

TABLE 1: Evaluation parameters obtained using AdaBoost of decision stump trees

Selection Method	SP	SE	ACC
Normal	0.79	0.86	0.82
Ensemble	0.77	0.95	0.85
OLA	0.77	0.95	0.85
LCA	0.67	0.92	0.79
A-Priori	0.72	0.95	0.82
A-Posterior	0.67	0.92	0.79
KNORA-E	0.74	0.95	0.84
KNORA-U	0.77	0.95	0.85

TABLE 2: Evaluation parameters obtained using decision stump Trees

Selection Method	SP	SE	ACC
Normal	0.74	0.84	0.79
Ensemble	0.70	0.97	0.82
OLA	0.72	0.95	0.82
LCA	0.67	0.92	0.79
A-Priori	0.70	0.95	0.81
A-Posterior	0.70	0.95	0.76
KNORA-E	0.70	0.92	0.80
KNORA-U	0.70	1.00	0.84

Using multilayer perceptron, sensitivity, specificity, and accuracy of 90.3%, 100%, and 95%, respectively is obtained. Figures 6 and 7 illustrate the confusion matrix for the corresponding ratios using the ANN classifier.

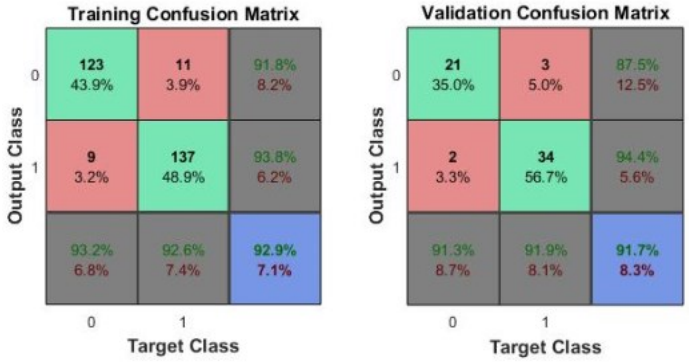

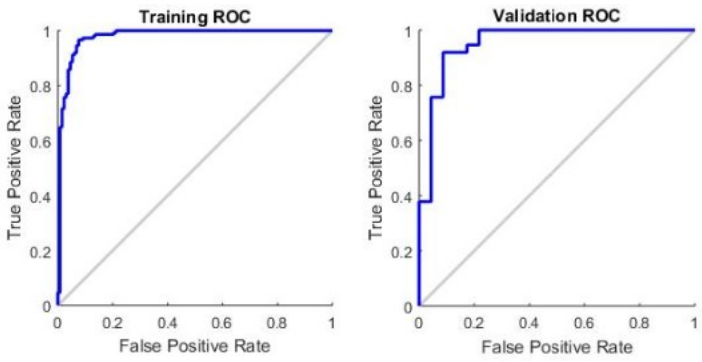

FIG. 6: Confusion matrix for training and validation classification along with corresponding ROC curve

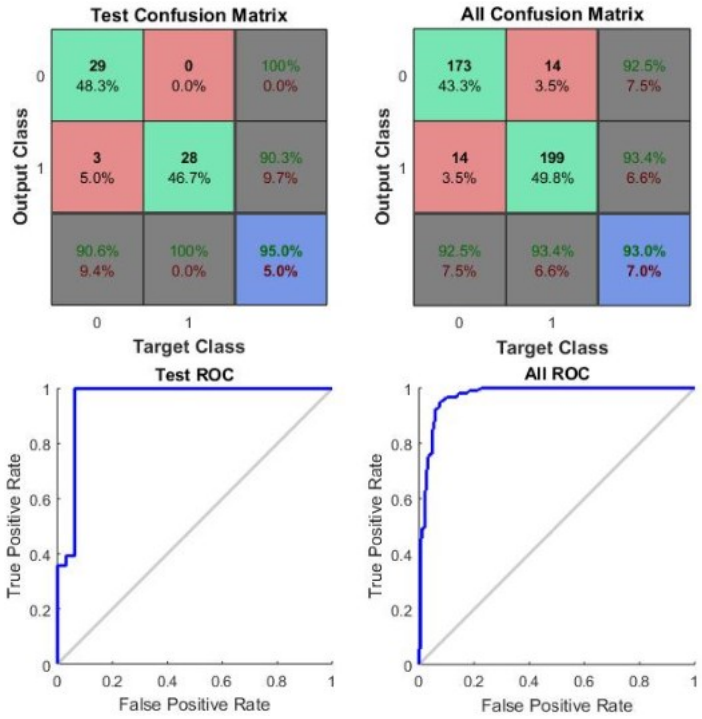

FIG. 7: Confusion matrix for testing and combine classification along with corresponding ROC curve

3.2 Results for Ensemble of Classifiers with Dynamic Selection Methods

Set-Up 2: The performance of OLA and KNORA-U dynamic selection techniques using AdaBoost of decision stump trees was better in comparison to the other dynamic

ensemble selection techniques. Similarly, in case of decision stump trees, KNORA-U dynamic ensemble selection technique resulted in good sensitivity, specificity and accuracy. The results for ensemble of classifiers are depicted in Tables 1 and 2.

4. CONCLUSIONS

A CAD tool for the diagnosis of pathological myopia is designed using three sequential steps. Novel algorithms for blood vessel detection and studying the shape characteristics of OD are proposed. The proposed set of features are quite few which efficiently aid in the detection of pathological myopia using a simple classifier architecture thus proving the efficacy of the extracted features. Since minimal number of features are used, the system complexity is reduced, resulting in decreased processing systems. The system can be adopted in clinical settings in rural areas where poor healthcare facilities are available for initial screening of myopic eyes.

REFERENCES

1. World Health Organization, (2018), *Meeting on Developing Myopia Control Strategies*, Singapore, Manila: WHO Regional Office for the Western Pacific.
2. Liu, J., Wong, D.W., Tan, N.M., Zhang, Z. et al., (2010) Automatic classification of pathological myopia in retinal fundus images using PAMELA, *Computer-Aided Diagnosis,* **7624**, pp. 766240G.
3. Zhang, Z., Cheng, J., Liu, J., Sheri, Y.C.M. et al., (2012) Pathological myopia detection from selective fundus image features, *7th IEEE Conference on Industrial Electronics and Applications*, pp. 1742-1745.
4. Zhang, Z., Xu, Y., Liu, J., Wong, D.W. et al., (2013) Automatic diagnosis of pathological myopia from heterogeneous biomedical data, *PLoS ONE*, **8**(6), pp. e65736.
5. PALM grand-challenge.org. https://palm.grand-challenge.org/ [Online Accessed - 18/04/2019].
6. Ohno-Matsui, K., (2017) What is the fundamental nature of pathologic myopia? *Retina*, **37**(6), pp. 1043-1048.
7. Marcus, M.W., de Vries, M.M., Montolio, F.G.J., and Jansonius, N.M., (2011) Myopia as a Risk Factor for Open-Angle Glaucoma: A Systematic Review and Meta-Analysis, *Ophthalmology*, **118**(10), pp. 1989-1994.
8. Yun, S.C., Hahn, I.K., Sung, K.R., Yoon, J.Y. et al., (2015) Lamina cribrosa depth according to the level of axial length in normal and glaucomatous eyes, *Graefes Arch Clin Exp Ophthalmol*, **253**(12), pp. 2247- 2253.
9. Mitchell, P., Hourihan, F., Sandbach, J., and Wang, J.Jin, (1999) The relationship between glaucoma and myopia: The blue mountains eye study, *Ophthalmology*, **106**(10), pp.2010-2015.
10. Liu, H., Li, L., Wormstone, I.M., Qiao, C. et al., (2019) Development and Validation of a Deep Learning System to Detect Glaucomatous Optic Neuropathy Using Fundus Photographs, *JAMA Ophthalmol*, **137**(12), pp. 1353-1360.
11. Otsu, N., (1979) A threshold selection method from gray-level histogram, *IEEE Transaction on System Man Cybernetics*, **9**(1), pp. 62- 66.
12. Chan, T.F. and Vese, L.A., (2001) Active contours without edges, *IEEE Transactions on Image processing*, **10**(2), pp. 266-277.
13. Ko, A.H., Sabourin, R., and Britto, Jr.A.S., (2018) From dynamic classifier selection to dynamic ensemble selection, *Pattern Recognition*, **41**(5), pp. 1718-1731.

14. Didaci, L., Giacinto, G., Roli, F., and Marcialis, G.L., (2005) A study on the performances of dynamic classifier selection based on local accuracy estimation, *Pattern Recognition*, **38**(11), pp. 2188-2191.
15. Bhatikar, S.R., DeGroff, C., and Mahajan, R.L., (2005) A classifier based on the artificial neural network approach for cardiologic auscultation in pediatrics, *Artificial intelligence in medicine*, **33**(3), pp. 251-260.